Journal of Visualization, Vol. 10, No. 4 (2007)349-357

Regular Paper

Qualitative Comparison between Numerical and Experimental Results of Unsteady Flow in a Radial Diffuser Pump

Feng, J.*, Benra, F.-K.* and Dohmen, H. J.*

* Department of Mechanical Engineering, Faculty of Engineering, University of Duisburg-Essen, Duisburg, 47048, Germany. E-mail: jianjun.feng@uni-due.de

Received 17 April 2007
Revised 27 August 2007

Abstract : Comparison between numerical simulation and experimental results for unsteady flow field in a radial diffuser pump is presented for the design operating point. The numerical result is obtained by solving three-dimensional, unsteady Reynolds-averaged Navier-Stokes equations by the commercial CFD code CFX-10 with $k-\omega$ based shear stress transport turbulence model. Two-dimensional PIV measurements are conducted to acquire the experiment result. The phase-averaged velocity and turbulent kinetic energy fields are compared in detail between the results by the two methods in the impeller, diffuser and return channel regions. The qualitative comparison between CFD and PIV results is quite good in the phase-averaged velocity field. Although the turbulence level by PIV is higher than that by CFD generally, the main turbulence features are nearly the same. Furthermore, the blade orientation effect and other associated unsteady phenomena are also examined, in order to enhance the understanding on impeller-diffuser interaction in a radial diffuser pump.

Keywords : Unsteady flow, PIV, CFD, Radial pump.

1. Introduction

For a radial pump equipped with a vaned diffuser, the impeller provides different inlet flow conditions for the diffuser during its rotation and the diffuser vanes also influence backwards the flow in the impeller. This interaction in between becomes very strong in the case of small radial gap and high density of the involved working fluid (Arndt et al., 1990). Some studies have been conducted numerically to investigate the unsteady velocity field in a radial diffuser pump, such as the work by Bert et al. (1996), He and Sato (2001), Ardizzon and Pavesi (2004), Benra and Dohmen (2005). Particle Image Velocimetry (PIV) appears to be an effective and non-intrusive experimental method to obtain the instantaneous velocity field, which has been conducted to measure the flow in a pump. Akin and Rockwell (1994) used PIV to study the wake from a model impeller and its interaction with diffuser vanes. Sinha et al. (2000) used PIV results to identify the unsteady flow structure and turbulence in a radial pump with a vaned diffuser. Wuibaut et al. (2002 and 2004) utilized PIV to measure the flow field in the impeller of a diffuser pump.

The above mentioned work contributes to the understanding of the complex unsteady flow due to impeller-diffuser interaction in diffuser radial pumps. However, the knowledge about this interaction needs to be enhanced. Compared to experiments, CFD (computational fluid dynamics) calculations can obtain more extensive results with less cost and time, but the numerical results should be validated by experiments to some extents. However, the comparison of unsteady velocity field between numerical simulation and experiment is scarce in the case of impeller-diffuser interactions, due to the difficulties in both (big grid size in numerical simulations and optical access constraints in experiments) and the possible bad agreement, especially for turbulence effects.

The unsteady flow field of a radial diffuser pump has been obtained both by CFD calculation and PIV measurement in this paper. The unsteady velocity and turbulent kinetic energy fields are analyzed and detailedly compared in the impeller and diffuser, and also in the return channel, which can enhance the understanding on impeller-diffuser interaction in radial diffuser pumps.

2. Nomenclature

b	mm	blade height	C	m/s	absolute velocity
K	m^2/s^2	turbulent kinetic energy	n	rpm	rotating speed
Q	m^3/h	volume flow rate	R	mm	radius
t	s	time	u	m/s	component in x-direction
v	m/s	component in y-direction	W	m/s	relative velocity
X	mm	x coordinate	Y	mm	y coordinate
Z	-	number of blades	φ	deg	rotating angle
θ	deg	angular coordinate	ω_z	1/s	vorticity

Subscripts

1	impeller inlet	2	impeller outlet
3	diffuser inlet	4	diffuser outlet
5	return channel inlet	6	return channel outlet
d	diffuser	des	design operating point
i	impeller	r	return channel

Superscripts

—	phase averaged	'	turbulent

3. Experiment and Numerical Simulation

3.1 Geometry of the Pump

The test pump stage consists of an impeller, a vaned diffuser and a vaned return channel. The impeller is shrouded with six strongly backswept blades. Both the diffuser and the return channel have nine vanes. All the blades are designed in two dimensions with constant thickness of 4 mm for the convenience of PIV measurements. The pump is driven by a motor with a maximum power of 45 kW, and the rotating speed can be increased softly and gradually from 0 to 50 Hz with a minimum step of 0.1 Hz. A tank with 3 m^3 pure water is used to feed the water into the pump and also recollect the water out of the pump. An electromagnetic flow meter is installed on the pipe behind the pump to measure the volume flow rate. The whole pump is manufactured with transparent glass, in order to provide optical access to the measuring region of interest for the laser sheet and camera. The geometric data and operating conditions are illustrated in Table 1. In addition, the measured characteristic curve of the pump is given in Fig. 1.

Table 1. Geometric data and operating conditions.

Number of impeller blades	Z_i	6	Number of return channel vanes	Z_r	9
Impeller inlet radius	R_1	40 mm	Return channel inlet radius	R_5	95 mm
Impeller outlet radius	R_2	75.25 mm	Return channel outlet radius	R_6	50 mm
Impeller width	b_i	12.7 mm	Return channel width	b_r	14 mm
Number of diffuser vanes	Z_d	9	Design flow rate	Q_{des}	0.0045 m^3/s
Diffuser inlet radius	R_3	77.5 mm	Design rotating speed	n_{des}	1450 rpm
Diffuser outlet radius	R_4	95 mm	Design delivery head	H_{des}	7 m
Diffuser width	b_d	14 mm	Specific speed	n_q	22.6

3.2 Experimental Set-Up

All the measurements in this paper are conducted at midspan, i.e., half blade height. An overview of the pump test stand is given in Fig. 2. The light source is a double-cavity 532 nm Nd-YAG laser with the repetition rate of 15 Hz and energy of 120 mJ/pulse. The laser beam in the diameter of 5 mm out of the laser system is guided by a flexible laser arm comprising a series of mirrored joints and hollow connecting tubes that totally enclose the high-energy pulsed laser beam. A cylindrical optics and a thickness adjuster are connected to the output end of the guiding arm. The optics produces a light sheet with a divergence angle of 15 deg and a thickness of approximately 1 mm in the area of interest, which is utilized to illuminate the particles added in the water. The water is seeded with powder particles in the average diameter of 20 µm. The powder has nearly the same density as water, so that the particles can follow the flow very well.

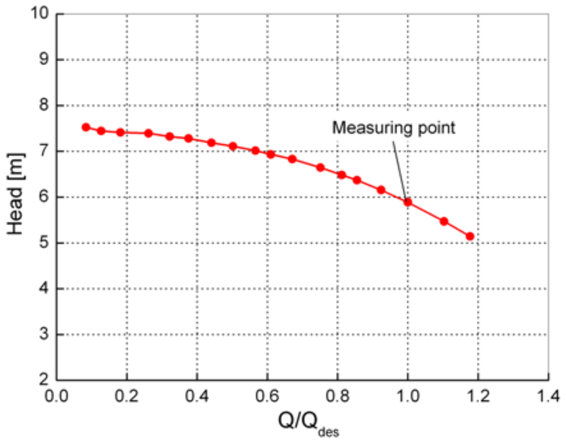

Fig. 1. Head curve of the pump stage.

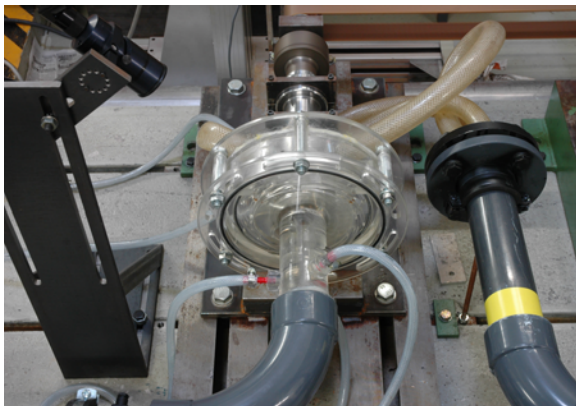

Fig. 2. Overview of the test stand.

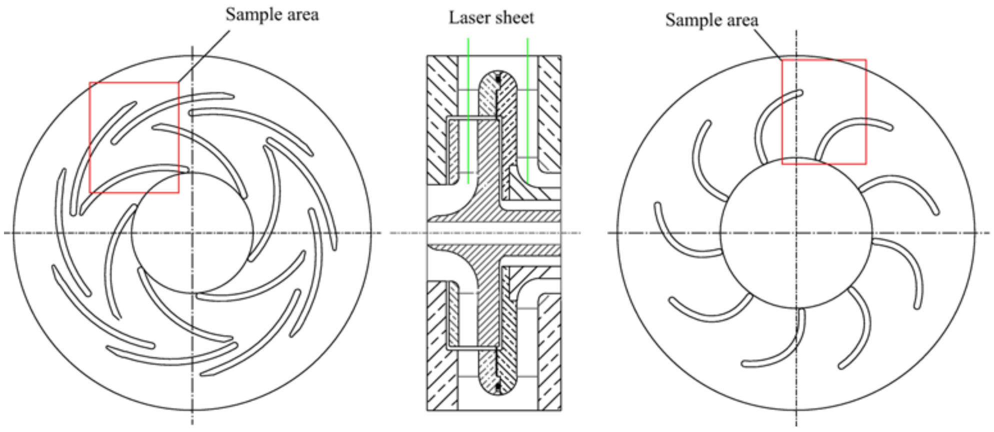

(a) (b)

Fig. 3. Sample areas for PIV : (a) in the impeller and diffuser and (b) in the return channel.

The images are recorded by a 1024 × 1280 pixels, 8-bit CCD (Charge Coupled Device) camera, which is aligned vertically to the laser sheet and mounted at a 2D traverse system. An optical filter is installed in front of the camera in order to avoid the laser light from reflections and to transmit only the fluorescent light from particles to the camera sensor. For each relative impeller position, 200 double-frame images are recorded. The time between two pulsed laser beams is set to 30 µs, corresponding to a rotating angle change of 0.26 deg under the design operating speed. Before the measurement, a predefined target with scales has been placed in the measuring area inside the pump with water, to get the scale factor between the object and the image. The sample areas are indicated in Fig. 3, which completely cover an impeller channel, a diffuser channel, and also a return channel, with the size of 58 mm × 72.5 mm in the impeller and diffuser region, and 55.1 mm × 68.9 mm in the return channel region. The laser and the camera are synchronized with the blade orientation by using a magnetic sensor installed on the pump shaft used as a shaft encoder. This sensor generates one pulse per revolution for the input of the PIV processor at a pre-selected impeller position. The other measuring position can be obtained by a time delay based on it. The measurements are conducted only in two dimensions, and the axial velocity is not measured. The adaptive correction is utilized to obtain a raw vector map for each double-image. The final interrogation size is 32 × 32 pixels with an overlap of 50 % in each direction. This data acquiring process provides 63 × 79 vectors for each image. Then a moving average method is utilized to smooth out the raw vector map with the averaging area of 3 × 3 vectors to validate vectors based on the comparison between neighboring vectors. A vector statistics function is further accomplished over the vector maps obtained at the same phase position, in order to calculate the phase-averaged velocity field and the standard deviations of the velocity components.

3.3 Numerical Simulation

Three-dimensional, unsteady Reynolds-averaged Navier-Stokes equations are solved by the CFD code CFX-10. The structured grid for computational domains is generated by using the commercial software ICEM-CFD 10 with multi-block templates, in which an O-Grid is created around the blade and an H-Grid is used in the blade passage. The O-Grid provides opportunities of excellent boundary layer resolutions. The impeller side chambers are also included in the grid to take leakage flow effects into account. The turbulence is simulated by $k-\omega$ based shear stress transport turbulence model (Menter, 1994) with 5 % turbulence intensity (the ratio between the fluctuating part and the mean velocity) and a viscosity ratio of 10 (the ratio between the turbulence viscosity and dynamic viscosity). Variations of these parameters do not show evident influences on the flow field. The interface between the impeller and the diffuser is set to “transient rotor-stator”, in which the relative position between the rotor and the stator is updated each time step. More details about the computational grid and boundary conditions can be taken from our previous work (Feng et al., 2007).

4. Results

All the results presented in this paper are limited to the design operating point Q_{des} and midspan. The measured velocity components (u and v) in two orthogonal directions (x and y) each can be decomposed into two parts: a phase-averaged component ($\bar{u}$ and $\bar{v}$) depending on the measuring point position and the impeller circumferential position, and a fluctuating component (u' and v') representing the turbulence effects, as denoted in Eqs. (1) and (2). The turbulence kinetic energy is calculated in Eq. (3) based on the turbulent components, and the Reynolds shear stress is also calculated in Eq. (4).

$$u(x,y,\theta,t)=\bar{u}(x,y,\theta)+u'(x,y,\theta,t)\,,\quad v(x,y,\theta,t)=\bar{v}(x,y,\theta)+v'(x,y,\theta,t) \tag{1}$$

$$\bar{u}(x,y,\theta)=\frac{1}{N}\sum_{i=0}^{N-1}u(x,y,\theta,t)\,,\ \bar{v}(x,y,\theta)=\frac{1}{N}\sum_{i=0}^{N-1}v(x,y,\theta,t) \tag{2}$$

$$K(x,y,\theta)=\frac{3}{2}\frac{1}{N}\sum_{i=0}^{N-1}\left[\frac{1}{2}u'^{2}(x,y,\theta,t)+\frac{1}{2}v'^{2}(x,y,\theta,t)\right] \tag{3}$$

$$\left|-\overline{u'v'}(x,y,\theta)\right|=\left|\frac{1}{N}\sum_{i=0}^{N-1}[u(x,y,\theta,t)-\bar{u}(x,y,\theta)][v(x,y,\theta,t)-\bar{v}(x,y,\theta)]\right| \tag{4}$$

Where N = 200 is the number of instantaneous vector maps for the same impeller position, θ is the impeller circumferential position. The factor 3/2 in Eq. (3) is to compensate for using only two velocity components available in the PIV data.

4.1 Flow in the Impeller and Diffuser

Figure 4 compares relative velocity contours obtained by CFD and PIV measurement with the same magnitude scale. The impeller rotation sense is clockwise. The qualitative agreement is quite good, and both predict nearly the same phenomena. For example, a positive incidence is found at the impeller leading edge, producing a local region near to the suction (concave) side with relatively high relative velocity. The adverse pressure gradients decelerate the flow from the leading edge to the trailing edge on the suction side. It is also observed that for both cases, the relative velocity on the suction side is bigger than on the pressure (convex) side in the front impeller part. However, this phenomenon is reversed in the impeller rear part due to the fact that the Coriolis force accumulates strength in large radiuses and drives the fluid from the suction side to the pressure side. Near the impeller outlet, a wake region characterized by low relative velocity is found on the impeller suction side near the trailing edge, and a local region with relatively high velocity on the corresponding pressure side. This kind of flow non-uniformity near the impeller outlet is the so-called jet-wake structure, which has been reported by Wuibaut et al. (2002). Concerning the flow in the diffuser region, the agreement is also quite good. Both predict the stagnation point and a negative incidence at the diffuser leading edge, a region with local high velocity on the pressure side near the diffuser leading edge, and the diffuser wake. In addition, the shapes of the velocity contours are quite similar.

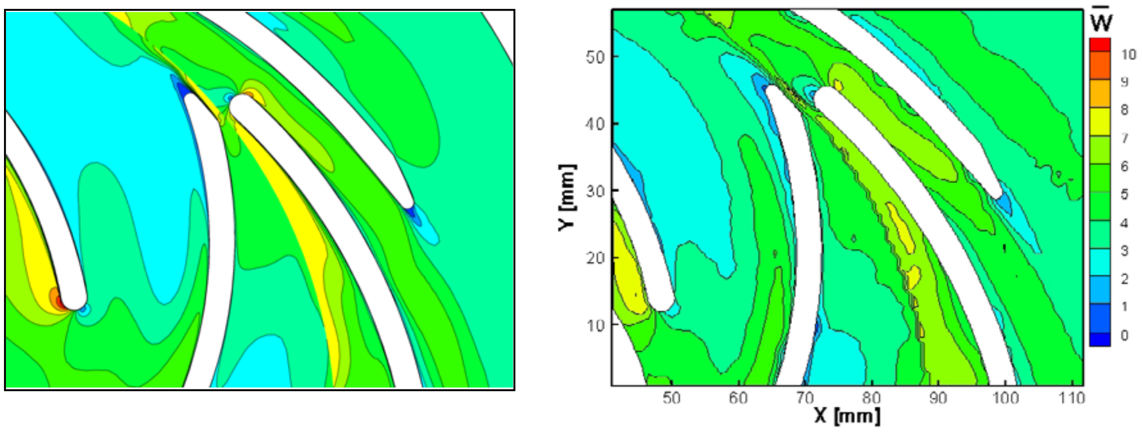

(a) By CFD (b) By PIV

Fig. 4. Comparison of relative velocity at $\varphi = 0$ deg.

Figure 5 shows the comparison of turbulent kinetic energy for one impeller position. Note that the scales are different: the magnitude for PIV result is bigger than that for CFD result for the same color, which means the turbulence for the PIV result is higher than that of CFD result. One reason is that the velocity fluctuations in PIV are not only caused by turbulence, but also by some other random errors in the measurement. Although there are some noises in the PIV result due to reflections, the main features can be easily identified. The CFD predicts high turbulence regions behind the impeller trailing edge, in the passage near the impeller inlet throat close to the impeller suction side due to the leakage flow in the front side chambers (confirmed by CFD by comparing the results between with and without consideration of side chambers), around the diffuser leading edge caused by impeller-diffuser interactions, and behind the diffuser trailing edge. Nearly all above high turbulence regions can be also observed in the result from PIV.

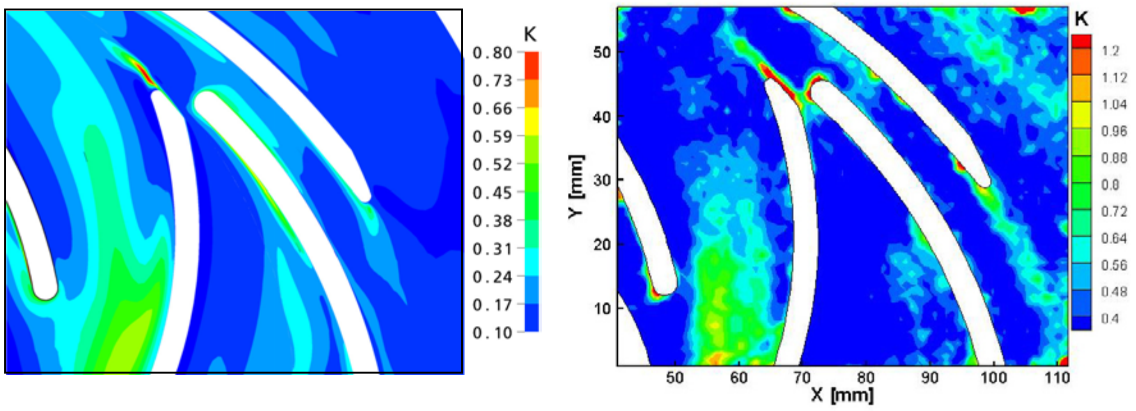

(a) By CFD (b) By PIV

Fig. 5. Comparison of turbulent kinetic energy at $\varphi = 0$ deg.

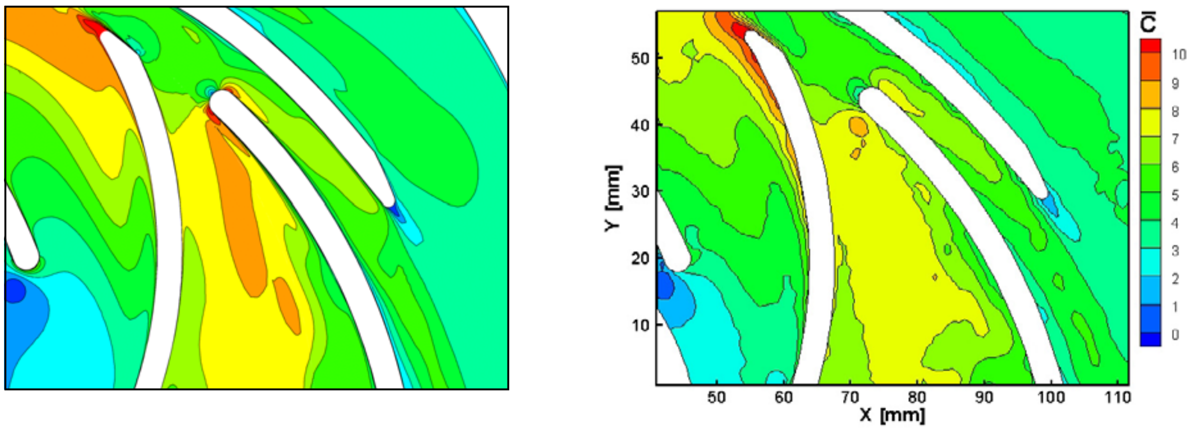

(a) By CFD, $\varphi = -10$ deg (b) By PIV, $\varphi = -10$ deg

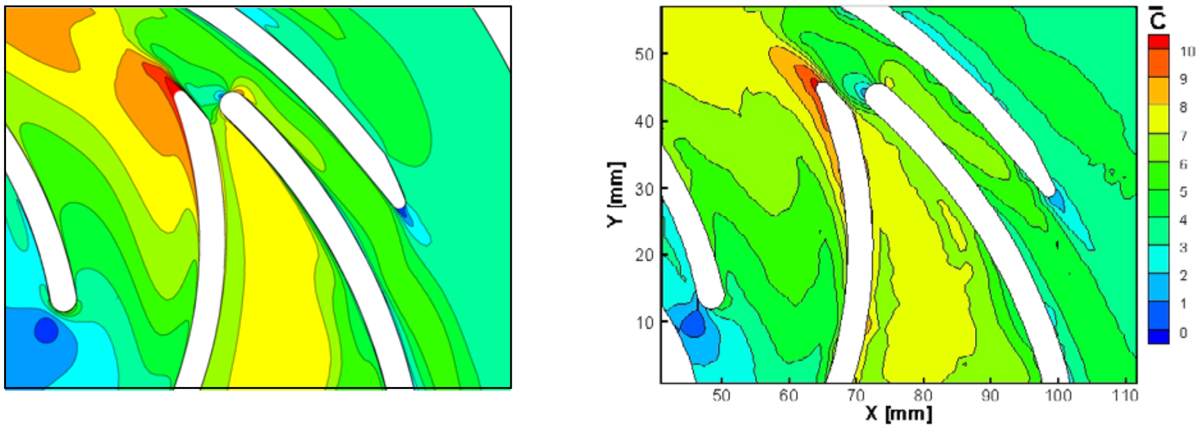

(a) By CFD, $\varphi = 0$ deg (b) By PIV, $\varphi = 0$ deg

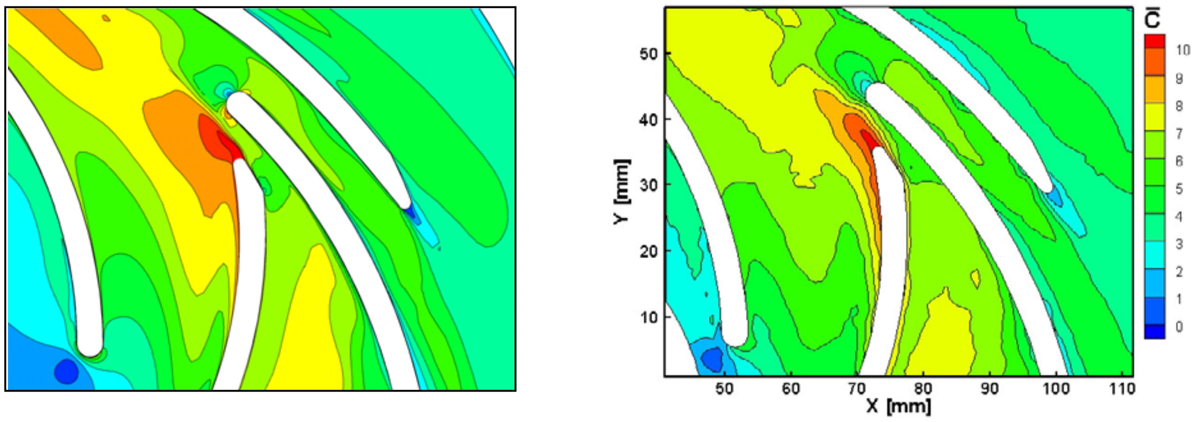

(a) By CFD, $\varphi = 10$ deg (b) By PIV, $\varphi = 10$ deg

Fig. 6. Phase-averaged absolute velocity distributions for three impeller positions.

The phase-averaged absolute velocity fields for three different impeller positions are presented in Fig. 6 both by CFD calculation and by PIV measurement with the same scale, in order to show the impeller rotation effects on the unsteady flow field. The comparison shows a very good agreement although the CFD slightly overestimates the velocities in some local small regions. It can be also observed in a qualitative manner that the presence of the diffuser vanes has only limited influence on the impeller inner velocity field, which has nearly the same behavior for all shown impeller positions. In the rear part near the impeller outlet, for all shown positions, a high absolute velocity zone is developed in the wake region near the impeller trailing edge on the suction surface, and this high velocity zone extends to the adjacent impeller pressure side. In addition, the extending high velocity region for CFD is bigger than that by PIV. Therefore, it can be concluded that the presence of the diffuser vanes has only a limited effect on the impeller inner flow structure, and the influence mainly confines to the flow field at the rear part of the impeller near the outlet. For all shown positions, a stagnation point is located on the leading edge and a wake region is found at the trailing edge, independently of the impeller positions. However, some striking differences in the flow can be observed in both results at the diffuser pressure side near the leading edge: the high velocity region due to the incidence changes during the impeller rotation. From $\varphi = -10$ to $\varphi = 10$ deg, this region decreases gradually then disappears, which is more evident in the CFD results, suggesting that the diffuser vane experiences different inlet flow conditions during the rotation of the impeller. There is a local low velocity region on the vane suction side for all positions in the region faced directly by the impeller trailing edge. In addition, it is found that the diffuser vane suction side is more influenced by the impeller position compared to the pressure side.

4.2 Flow in the Return Channel

Figure 7 illustrates the comparisons of absolute velocity in the return channel at $\varphi = 0$ deg with the same scale. The CFD predicts a big separation zone on the pressure (convex) side of the return channel vane, which can also be observed in the result provided by PIV, especially by the streamlines. This flow separation is due to the fact that the vanes are designed to give a swirl free inflow for the next stage. Since the absolute flow leaves the diffuser with a small flow angle, the return channel vanes have to turn the flow by more than 70 deg for the purpose of design mentioned above. This strong flow turning is responsible for the flow separation. Furthermore, the starting position and the size of the separation zone by CFD are in a very good agreement with those by PIV. Near the vane trailing edge, the CFD overestimates the velocity compared with PIV. By checking the images with particles captured by the camera, this could be explained that there are not enough particles due to the shadows near the sampling border in the PIV measurement. Furthermore, by comparing the velocity field for different impeller rotating angles, it is found that the impeller rotation has nearly no influence on the velocity field in the return channel. This is because the impeller orientation effects on the velocity field have vanished before reaching the return channel region due to the long meridional distance.

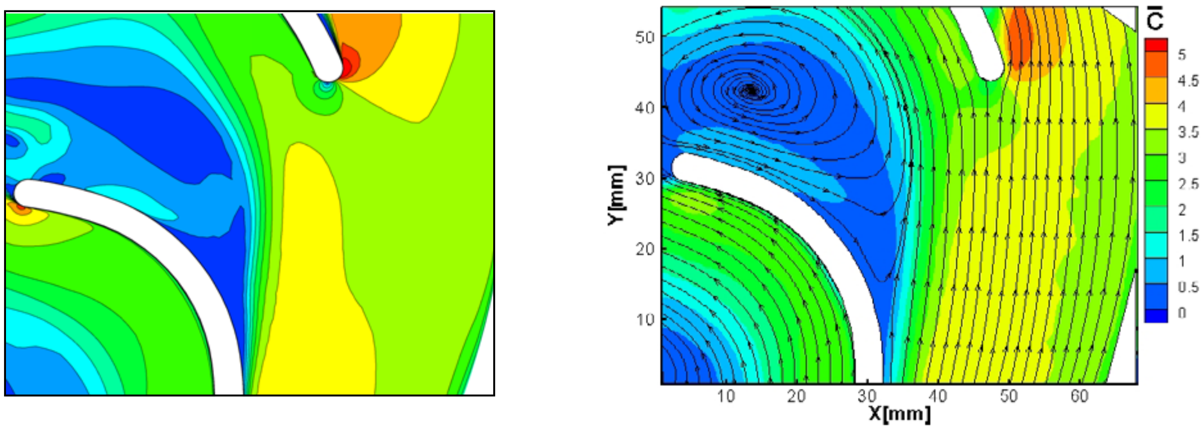

(a) By CFD (b) By PIV

Fig. 7. Comparison of phase-averaged absolute velocity in the return channel at impeller rotating angle $\varphi = 0$ deg.

Figure 8 presents the comparison of turbulence kinetic energy in the return channel for $\varphi = 0$ deg. The turbulence level by PIV is much higher than that by CFD, since the magnitude for PIV result is 10/3 times bigger than that of CFD result for the same color in the contour. However, the phenomena are quite similar: a high turbulence region shedding from the vane pressure side just before the start position of the flow separation, and the region around the vane leading edge. There is another high turbulence region in CFD result near the vane trailing edge which has not been captured by PIV possibly due to the shadows in the image mentioned above.

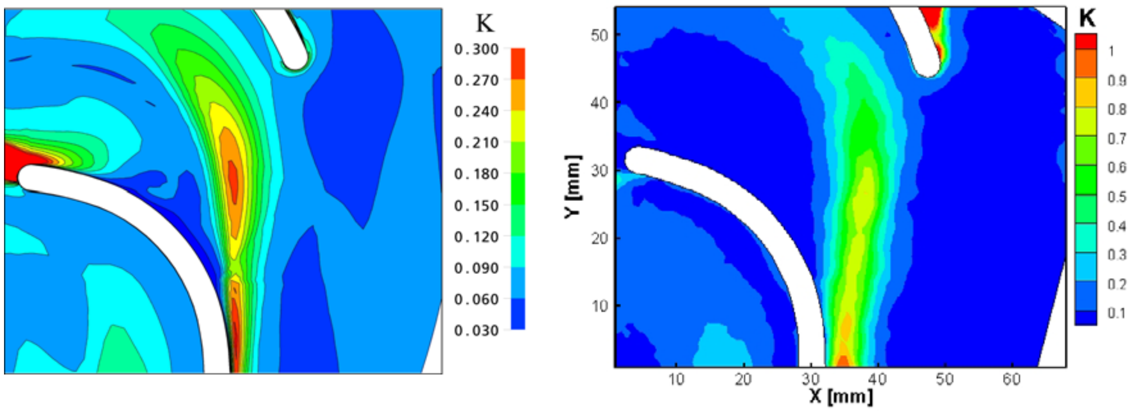

(a) By CFD (b) By PIV

Fig. 8. Comparison of turbulent kinetic energy in the return channel at $\varphi = 0$ deg.

Figure 9 presents the Reynolds shear stress and vorticity in the return channel at $\varphi = 0$ deg by PIV measurement.It is found that both have the similar distribution to the turbulent kinetic energy shown in Fig. 8(b): the regions with high magnitude shedding from the vane pressure side just before the start position of the flow separation, and around the vane leading edge. For the Reynolds shear stress, it is totally in accordance with turbulent kinetic energy, suggesting that the two velocity components (u and v) are strongly correlated. There is another high vorticity region near the vane suction side.

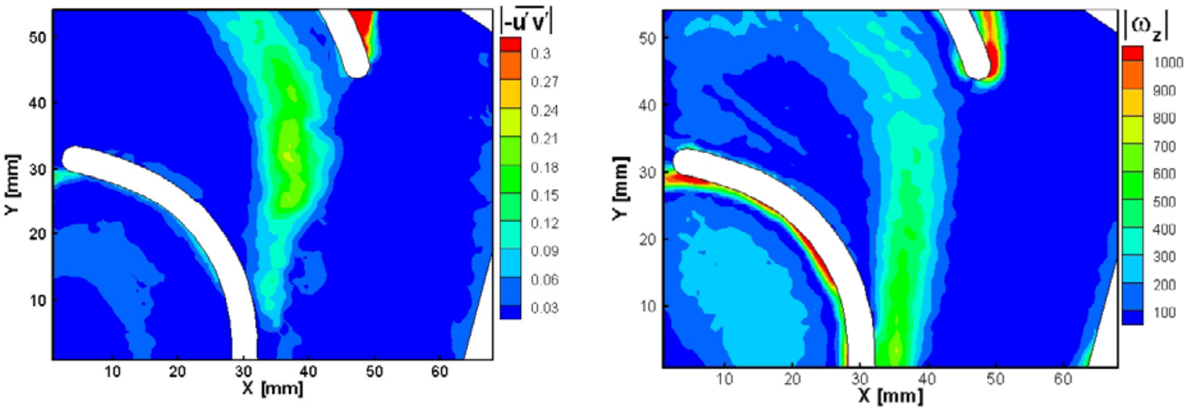

(a) (b)

Fig. 9. Reynolds shear stress (a) and vorticity (b) in the return channel at $\varphi = 0$ deg by PIV.

5. Conclusion

The periodic velocity flow field of a radial diffuser pump has been obtained both by PIV method and by CFD calculation. The unsteady velocity and turbulent kinetic energy fields are compared in between in the impeller, diffuser and return channel regions. The followings can be concluded:

(1) The qualitative agreements in velocity field are quite good in all shown positions in the impeller, diffuser, and return channel. Although the turbulence level by PIV is higher than that by CFD in the whole field, the main features are quite similar: high turbulence regions are located behind the impeller trailing edge, in the passage near the impeller inlet throat close to the impeller suction side, around the diffuser leading edge, and behind the diffuser trailing edge.

(2) A jet-wake flow structure is observed near the impeller outlet for all impeller positions.

(3) The influence on the impeller flow field from the presence of the diffuser vanes mainly confines to the rear part of the impeller near the outlet.

(4) The diffuser flow strongly depends on the relative impeller position which provides different inflow conditions for the diffuser. Compared to the pressure side, the diffuser

suction side is more influenced by the non-uniform flow out of the impeller.

(5) Flow separation has been found on the pressure side of the return channel vane. The velocity field in the return channel is nearly independent of the impeller rotation. High turbulence regions are observed on vane pressure side just before the start position of the flow separation around the vane leading edge.

References

Akin, O. and Rockwell, D., Flow Structure in a Radial Flow Pumping System Using High-Image-Density Particle Image Velocimetry, ASME Journal of Fluids Engineering, 116 (1994), 538-554.

Ardizzon, G. and Pavesi, G., Analysis of Unsteady Flow in a Vaned Diffuser Radial Flow Pump, The 10th International Symposium on Transport Phenomena and Dynamics of Rotating Machinery (Honolulu, Hawaii, USA), (2004-3).

Ardizzon, G. and Pavesi, G., Analysis of Unsteady Impeller Diffuser Interaction in a Centrifugal Pump, 22nd IAHR Symposium on Hydraulic Machinery and Systems (Stockholm, Sweden), (2004-6,7).

Arndt, N., Acosta, A. J., Brennen, C. E. and Caughey, T. K., Experimental Investigation of Rotor-Stator Interaction in a Centrifugal Pump with Several Vaned Diffusers, Journal of Turbomachinery, 112 (1990), 98-108.

Benra, F.-K. and Dohmen, H. J., Numerical Investigation of the Transient Flow in a Centrifugal Pump Stage, 2005 ASME Fluids Engineering Division Summer Meeting and Exhibition (Houston, TX, USA), (2005-6).

Bert, P. F., Combes, J. F. and Kueny. J. L., Unsteady Flow Calculation in a Centrifugal Pump Using a Finite Element Method, XVIII IAHR Symposium on Hydraulic Machinery and Cavitation (Valencia, Spain), (1996-9).

Feng, J., Benra F.-K. and Dohmen. H. J., Numerical Investigation on Pressure Fluctuations for Different Configurations of Vaned Diffuser Pumps, International Journal of Rotating Machinery, (2007), 1-10.

He, L. and Sato, K., Numerical Solution of Incompressible Unsteady Flows in Turbomachinery, ASME Journal of Fluids Engineering, 123 (2001), 680-685.

Menter, F. R.. Two-equation Eddy-viscosity Turbulence Models for Engineering Applications, AIAA-Journal, 32 (1994), 269 -289.

Sinha, M. and Katz, J., Quantitative Visualization of the Flow in a Centrifugal Pump with Diffuser Vanes. Part I: On flow structures and turbulence, ASME Journal of Fluids Engineering, 122 (2000), 97-107.

Wuibaut, G., Bois, G., Dupont, P., Caignaert, G. and Stanislas, M., PIV Measurements in the Impeller and the Vaneless Diffuser of a Radial Flow Pump in Design and Off-design Operating Conditions, ASME Journal of Fluids Engineering, 124 (2002), 791-797.

Wuibaut, G., Bois, G., Dupont, P. and Caignaert, G., Rotor Stator Interactions in a Vaned Diffuser of a Radial Flow Pump for Different Flow Rates Using PIV Measurement Technique, 9th International Symposium on Transport Phenomena and Dynamics of Rotating Machinery (Hawaii, USA), (2002-9).

Wuibaut, G., Dupont, P., Caignaert, G. and Bois, G., Rotor Stator Interactions in a Vaned Diffuser Radial Flow Pump, 22nd IAHR Symposium on Hydraulic Machinery and Systems (Stockholm, Sweden), (2004-6,7).

Author Profile

Jianjun Feng: He received his Master-degree from Xi'an University of Technology in 2002. Then he was a Ph.D student in Xi'an Jiaotong University in China. Since late 2003, He works as a scientific employee in the chair of Turbomachinery in University of Duisburg-Essen in Germany. His main scientific interests are impeller-diffuser interactions, including CFD calculations and flow measurements by PIV and LDV.

Prof. F.-K. Benra: He received his PhD-degree from the Turbomachinery Institute of University Duisburg in 1986. Currently he holds the chair of Turbomachinery in University of Duisburg-Essen. His main scientific interests are rotor-stator interaction and fluid-structure interaction in all kinds of turbomachines and flow and heat transfer phenomena in secondary air systems of gas turbines.

Hans Josef Dohmen: He received his PhD-degree from the Turbomachinery Institute of University Duisburg in 1989. His main scientific interests are rotor-stator interaction and fluid-structure interaction in all kinds of turbomachines and flow and heat transfer phenomena in secondary air systems of gas turbines.